Chapter 7

Observation of the topological Hall effect and signature of skyrmions in high Curie-temperature Co_2FeAl Heusler compound

This work is authored by Gaurav K. Shukla et al.(To be submitted)

In this chapter, we report the topological Hall effect (THE) in the bulk Co_2FeAl Heusler compound. The observed THE is related to the skyrmion texture in the material, which is further confirmed by the ac-susceptibility measurements and micromagnetic simulations.

7.1 Introduction

Ever-demanding information and communication technologies necessitate the exploration of novel materials to enhance the functionality of their components. In recent advancements, the utilization of topological non-trivial spin structures has attracted immense attention for technological applications like next-generation spintronics devices and ultra-fast information technology [1–4]. The topological Hall effect (THE) serves as an effective tool to detect the non-trivial spin texture in the materials [5–7]. THE emerges as a consequence of real space Berry curvature that an electron acquires while traversing through the non-trivial spin texture of the material [8–10]. This acquisition results in an additional contribution in Hall resistivity, giving rise to the observed phenomenon of THE [11–13]. An interesting example of a non-trivial spin texture is magnetic skyrmions, which are topologically protected nano-domain magnetic structures and have created considerable interest as they can be driven at very low current density through spin-orbit torque mechanism [14–17]. The magnetic moment at the core points of the skyrmion is anti-parallel to the external magnetic field and parallel at the periphery [18]. The whole magnetic moment of the skyrmion wraps a sphere and gives rise to the topological charge ± 1, which makes ensure particle like the feature of skyrmion [18, 19]. The skyrmions were initially identified in non-centrosymmetric materials, where the lack of inversion symmetry of crystal lattice induces finite Dzyaloshinskii–Moriya interaction (DMI) via spin-orbit coupling. For e.g. MnSi[20], FeGe [21], FeCoSi [22] and thin-films heterostructure [23–26], Heusler alloys [27–31] exhibit skyrmion due to the finite DMI.

In recent discoveries, the formation of the skyrmionic structure is not restricted to non-centrosymmetric materials. In the centrosymmetric system, the skyrmions might be encountered due to the frustrated exchange interactions [32] or the competition among the long-range dipolar interaction, magnetic anisotropy, and exchange interactions. For e.g., the centrosymmetric materials Mn_4Ga_2Sn [33], Fe_3Sn_2 [34, 35], Gd_2PdSi_3 [36, 37], $La_{(1-x)}Sr_xMnO_3$ [18], Fe-Gd multilayer film [38], Fe_3GeTe_2 [39], etc. are reported to have the skyrmionic structure due to different competing magnetic inter-

actions. It is worthwhile to mention here that in contrast to the DMI stabilized skyrmions with fixed chirality in the non-centrosymmetric materials, the centrosymmetric systems often exhibit magnetic skyrmion bubbles with vorticity and helicity and hence the chirality can be manipulated through stimuli [39, 40]. Heusler compounds are a prominent class of materials due to their wide range of technological properties [41–43]. Recently the centrosymmetric Heusler compounds are also being reported to have skyrmions, such as Ni_2MnGa [44], NiMnGa [13, 45], $(Mn_{1-x}Ni_x)_{65}Ga_{35}$ [40], and NiMnX (X=In, Ga) [46], etc. Co_2FeAl, a centrosymmetric Heusler compound exhibits a significant degree of spin-polarization [47], low damping factor [48], and large Curie temperature [49], which are favorable conditions for spintronic device application. Additionally, two independent studies have shown the existence of skyrmions in thin films or layers of Co_2FeAl, attributing their formation to the interfacial Dzyaloshinskii-Moriya interaction (DMI) [23, 50]. We aim to investigate the existence and behavior of skyrmions in bulk Co_2FeAl, specifically focusing on a scenario where the influence of the Dzyaloshinskii-Moriya interaction (DMI) is disregarded.

This work presents indirect evidence of skyrmion in bulk Co_2FeAl using magnetotransport and AC-χ(H) measurements, along with micromagnetic simulations. The transport measurement reveals the presence of THE in a broad temperature range of 2 K to 300 K, and the maximum topological Hall resistivity is about 0.22 $\mu\Omega$-cm at 300K. The THE shows nearly temperature-independent behavior, which indicates its correlation with the real space Berry curvature originating from the skyrmionic phase present in the system. Micromagnetic simulation suggests that the skyrmionic bubble arising from competition among the magnetic anisotropy, exchange interaction, and long-range dipolar interaction energy gives rise to THE in the system.

7.2 Result and discussion

7.2.1 Sample preparation and characterization method

The sample preparation and characterization methods for the present compound can be found in Chapter 4.

7.2.2 Magnetization and magnetoresistance measurements

Figure 7.1(a) shows magnetic isotherms at different temperatures (between 2K to 300K) up to ± 7 T of the applied magnetic field. The saturation magnetization is 5.75 μ_B/f.u. at 2 K and 5.50 μ_B/f.u. at 300 K, which are close to the reported in literature [49, 51, 52]. To ascertain the temperature at

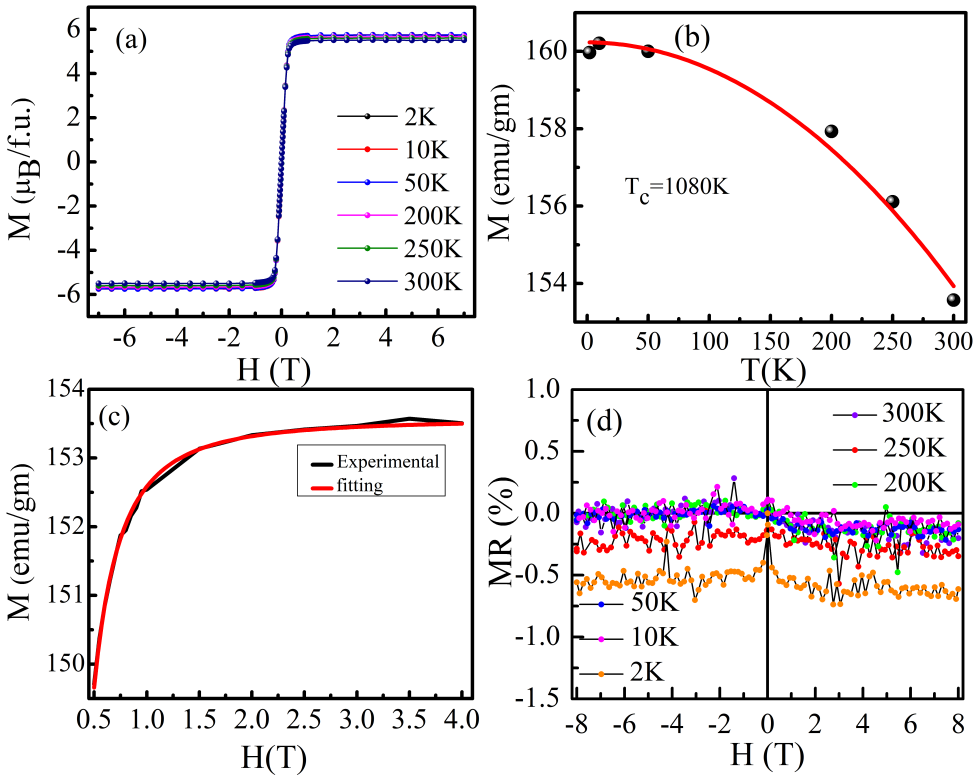

Figure 7.1: (a) Field-dependent magnetic isotherms *M(H)* at different temperatures. (b) Saturation magnetization M_s versus T data (black color) and the fitting is shown in red color. (c) M versus H data (black color) and the fitting using the Eq.7.1 is shown in red color. (d) Field variation of MR% at different temperatures.

which Curie transition occurs, we have plotted saturation magnetization M_s versus T data (black color) in Fig. 7.1(b) and fitted the data using an empirical relation $M_s = M_0[1 - (\frac{T}{T_c})^2]^{1/2}$ [53], where T_c is the Curie temperature. By fitting [red curve in Fig. 7.1(b)], we found T_c about 1080 K for the present compound, which is comparable to the reported in literature [54]. It is well established in the literature that magnetic anisotropy plays a pivotal role in skyrmion formation in the centrosymmetric system [33, 46, 55], we utilize "Law of approach to saturation" [56] to calculate magnetic anisotropy, expressed as follows;

$$M(H) = M_0(1 - \frac{A}{H^2}) \tag{7.1}$$

where $M(H)$ is the field-dependent magnetization of the material. In Fig. 7.1 (c) we have plotted high field $M(H)$ data (black curve) and fitted this using Eq.7.1 (red curve) to find out the value of constant A. We calculated the value of magnetic anisotropy (K) by using relation $A = \frac{8}{105}(K^2/{M_0}^2)$ [56] and found K about 0.3 MJ/m^3 at 300K, which is in the same order as reported in the literature [23, 50, 57]. The magnetoresistance (MR%) was calculated using the formula $MR(\%) = \frac{\rho(H)-\rho(0)}{\rho(0)} \times 100\%$, where ρ(H) is the longitudinal resistivity at field H and $\rho(0)$ is the zero field longitudinal resistivity. It is worthwhile to mention here that the field-dependent ρ_{xx} data was symmetrized with respect to the field direction [*i.e* $\rho_{xx} = \frac{\rho_{xx}(+H)+\rho_{xx}(-H)}{2}$] to subtract the Hall component from ρ_{xx}. The field variation of MR at different temperatures is shown in Fig.7.1(d). The MR% of about 0.48% and 0.13% were found at 2 K and 300 K, respectively. The values of MR% are small because ρ_{xx} remains nearly constant in response to changes in the magnetic field.

7.2.3 Topological Hall effect

The field-dependent Hall resistivity data in the temperature range of 2 K to 300 K is shown in Fig.7.2(a). Hall resistivity is given by equation [58]

$$\rho_{xy}(H) = R_0 H + R_s M + \rho^T, \tag{7.2}$$

where $R_0 H$ is the normal Hall resistivity and $R_s M$ is the anomalous Hall resistivity [49, 59, 60] and the last term ρ^T is topological Hall resistivity induced by the non-trivial spin texture of the sample. The factor R_s is weakly magnetic field dependent term[61–63]. The $R_s M$ can be simplified as $R_s M = S_A \rho_{xx}^2 M$, where S_A is a factor independent from the magnetic field and propositional to spin-orbit coupling[13, 64]. Thus, Eq.7.2 can be expressed as $\rho_{xy}(H) = R_0 H + S_A \rho_{xx}^2 M + \rho^T$. At the higher magnetic field magnetization reaches its saturation point *i.e.* all the spins are aligned in the same direction which results in the vanishing ρ^T due to the absence of spin texture. Therefore, at high field region intercept and slope of linear fitting between $\frac{\rho_{xy}}{H}$ and $\frac{\rho_{xx}^2 M}{H}$ gives R_0 and S_A, respectively. The values of R_0 and S_A are given in Table 7.1. The negative value of R_0 suggests electron-like conduction in the sample. Using the obtained values of R_0 and S_A, we calculated the Hall resistivity

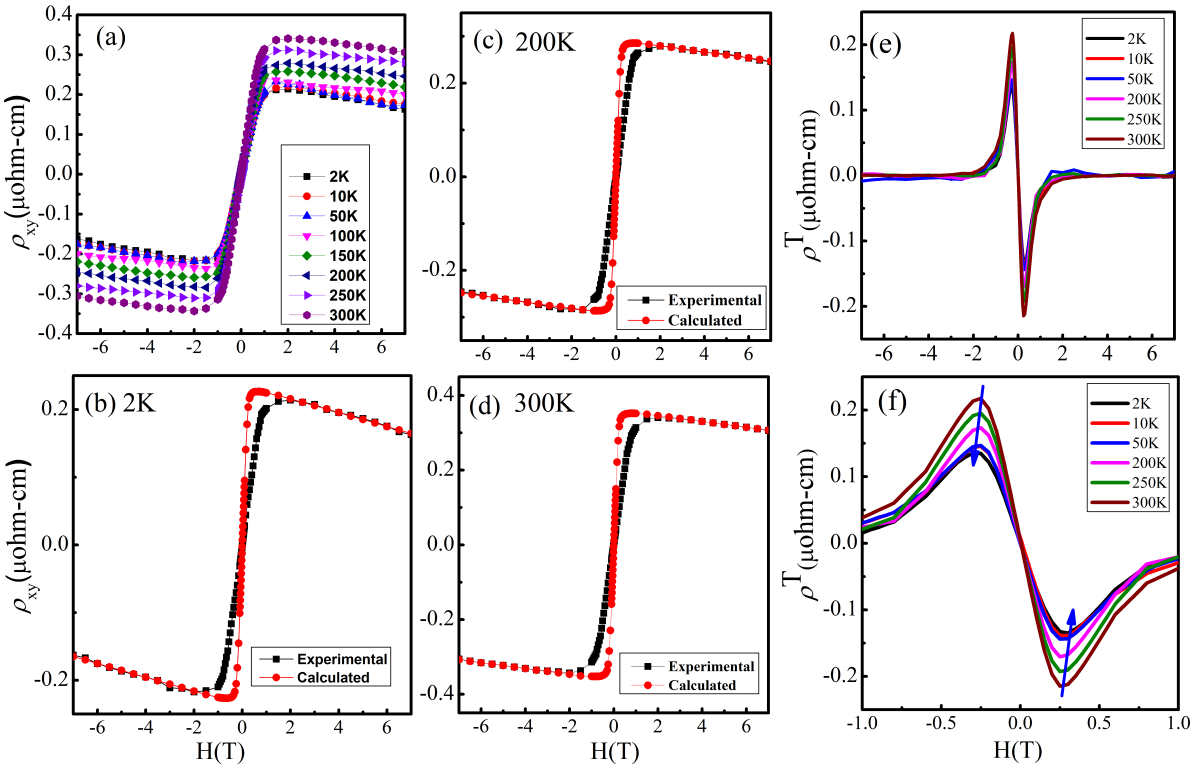

Figure 7.2: (a) Hall resistivity ρ_{xy} at the different temperatures. Experimental (black curve) and calculated Hall resistivity (red curve) for (b) 2 K (c) 200 K (d) 300 K. (e) Field-dependent topological Hall resistivity at different temperatures. (f) An enlarged view of topological Hall resistivity around ± 1 T.

using the relation

$$\rho_{xy}^{calc} = R_0 H + S_A \rho_{xx}^2 M \tag{7.3}$$

The difference between the experimental and calculated Hall resistivity gives the value of ρ^T. In Fig.7.2(b),(c),(d) we have plotted the experimental (black curve) and calculated Hall resistivity (red curve) at 2 K, 200 K, and 300 K, respectively. We can clearly see the difference between the experimental and calculated Hall resistivity at the low-field region. The values of ρ^T (ρ_{xy} - ρ_{xy}^{calc}) at various temperatures are given in Table 7.1.

Figure 7.2(e) summarizes the variation of ρ^T with magnetic field at various temperatures. We found that THE stabilizes in all temperature ranges (2 K to 300 K) and the peak value of ρ^T increases rather slowly with increasing temperature. The maximum ρ_{max}^T = -0.22 $\mu\Omega$-cm was found at 300 K. To achieve maxima in ρ^T, the required magnetic field is slightly increasing with decreasing the temperature as guided by the blue arrow in Fig. 7.2(f). This suggests that the magnetic field required to induce maximum THE is a function of temperature. A similar feature has been reported for

Tem (K)	R_0 (μohm-cm/T)	S_A (gm/ohm-m-emu)	ρ^T ($\mu\Omega$-cm)
2	-0.0107	141.74	-0.13
10	-0.0093	142.71	-0.14
50	-0.0116	144.68	-0.14
200	-0.0065	133.5	-0.17
250	-0.0054	135	-0.19
300	-0.0074	142.74	-0.22

Table 7.1: Value of R_0, S_A and ρ^T at various temperatures.

THE in skyrmion hosting materials [13, 64]. In addition to this, the magnitude of ρ^T is nearly T-independent in a broad temperature range, which suggests its association with the real space Berry curvature originated from the skyrmionic texture in the system [65].

7.2.4 AC-susceptibility measurement

It is widely recognized that the field evolution of skyrmion is accompanied by the hump/dip anomaly in AC-susceptibility (AC-$\chi(H)$) measurements. The DC magnetization measurement is sensitive to the sample magnetization, while the AC-$\chi(H)$ measurement is sensitive to the change in magnetization with field variation and hence gives the magnetization dynamics [66]. To check the similar type of features in the present system, we performed four-loops AC-$\chi(H)$ measurement in the field range of ± 1 T and the temperature range of 2 K to 300 K. The results are depicted in Fig. 7.3(a) with a y-axis offset for clarity. The AC-$\chi(H)$ decreases monotonically with an increase in the magnetic field. It shows a small hump around ± 0.2 T as shown by the arrows in Fig.7.3(a). Furthermore, Fig.7.3(a) clearly shows hysteresis in field-dependent AC-$\chi(H)$ data at different temperatures. To enhance the clarity of the hump/dip anomaly, we have included enlarged plots of the AC-$\chi(H)$ at 300 K, 250 K, 50 K, and 10 K in Fig. 7.3(b)[(i)-(iv)]. The detection of the hump-like anomaly in the AC-$\chi(H)$ suggests the existence of skyrmion texture in the present sample. Interestingly, the hump in AC-$\chi(H)$ aligns with the magnetic field, where THE reaches its maximum value. It is worthwhile to mention here that the hump-like feature in magnetic field-dependent AC-$\chi(H)$ measurement has been observed in the skyrmion host materials and can be used as a tool to indirectly probe the skyrmions in the systems [33, 64, 67–69]. Figure 7.3(c) displays the derivative of AC-$\chi(H)$ at different temperatures, offset along the y-axis for clarity. The sharp changes in the

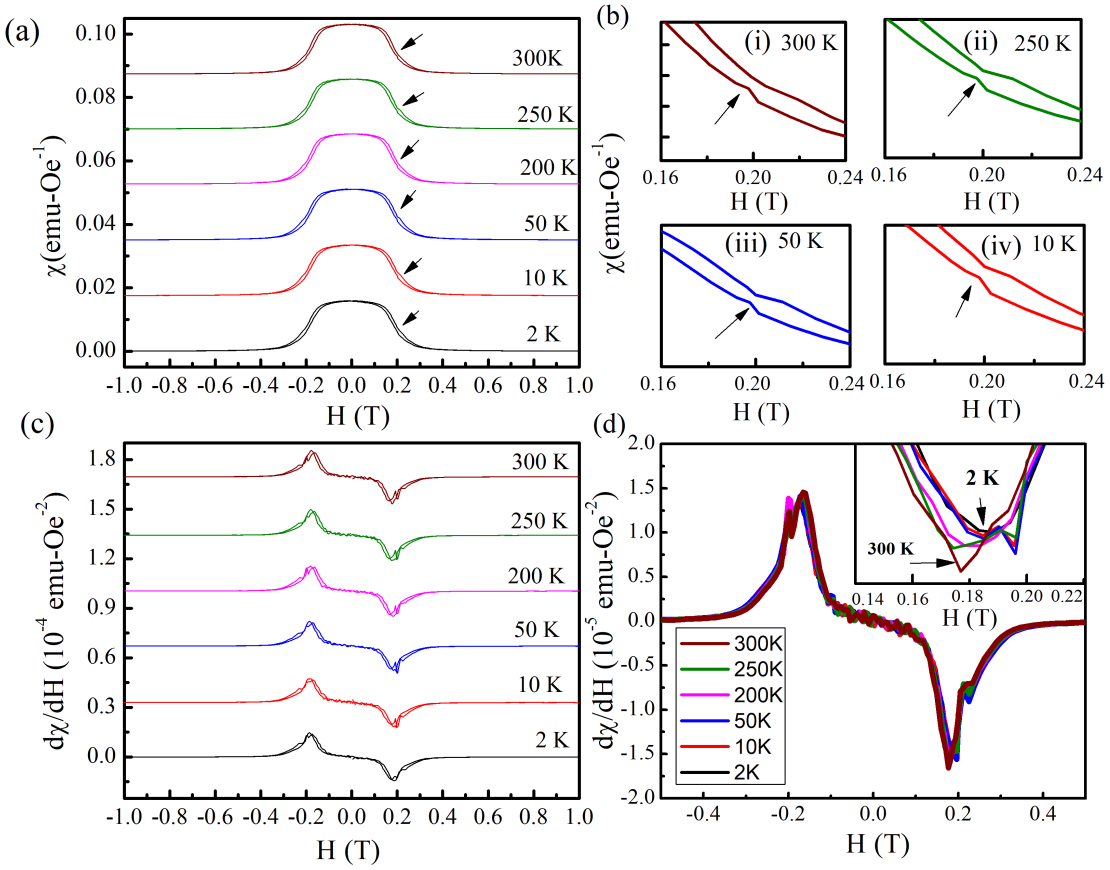

Figure 7.3: (a) Field-dependent AC-$\chi(H)$ at different temperatures plotted with an offset along the y-axis. The arrows indicate the hump in the AC-$\chi(H)$. (b) The enlarged view of the AC-$\chi(H)$ at (i) 300 K (ii) 250 K (iii) 50 K and (iv) 10 K. The arrows indicate the hump in the AC-$\chi(H)$ data. (c) Derivatives of AC-$\chi(H)$ at the different temperatures plotted with an offset along the y-axis. (d) The derivative of the AC-$\chi(H)$ at different temperatures (without offset) from 0.5T to -0.5 T. The inset shows the enlarged view around 0.2 T.

derivatives of AC-$\chi(H)$ occur around ± 0.2 T, and are the result of hump/dip anomaly present in the AC-$\chi(H)$ data. The sharp change around ± 0.2 T displays hysteresis behavior during both increasing and decreasing magnetic field cycles, which shows nucleation and annihilation of skyrmionic texture with increasing and decreasing field. This kind of hysteretic behavior for the formation of skyrmionic (anti) texture has been reported for $Mn_{1.4}PtSn$ Heusler alloy [68]. This suggests that THE observed in the present system is linked with the potential skyrmion phase in the material. In Fig. 7.3(d), we once again present the two-cycle derivative of AC-$\chi(H)$ spanning from +0.5 T to -0.5 T, this time without any y-axis offset. Inset within Fig. 7.3(d) provides an enlarged view around 0.2 T, revealing that the peak value of the AC-$\chi(H)$ derivative at 300 K surpasses that at 2 K, as indicated by the arrows. This observation correlates with the behavior of ρ^T, which attains

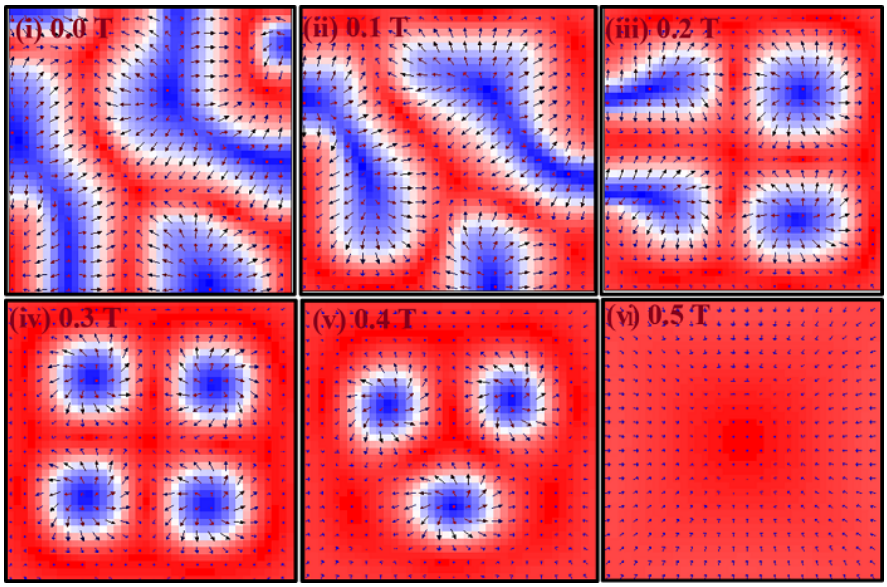

Figure 7.4: Different equilibrium magnetic states (top view) at the magnetic field values (i) 0 T (ii) 0.1 T (iii) 0.2 T (iv) 0.3 T (v) 0.4 T (vi) 0.5 T magnetic fields. The magnetization (m_z) is depicted using red color for positive values (+m_z) and blue color for negative values (-m_z), while in-plane magnetization is illustrated by a white region surrounded by blue features.

its maximum value at 300 K, slightly exceeding that at 2 K.

7.2.5 Micromagnetic simulation

Motivated by field-induced hump-like signature in $\chi(H)$ data, we conducted the micromagnetic simulation to investigate the presence of skyrmionic phase in the system. For the present system, micromagnetic simulations were conducted using the 3D object-oriented micromagnetic framework (OOMMF) code, employing the LLG function[70]. The slab geometry of dimensions 400 nm $\times$ 400 nm $\times$ 80 nm was used for the simulation with a grid of dimensions 10 nm $\times$ 10 nm $\times$ 4 nm. We have used the saturation magnetization M_s and magnetic anisotropy K about 1.1MA/m and 0.3 MJ/m^3 as found from the experiment. The exchange stiffness constant (A_{ex}) was estimated using formulae $A_{ex} \approx \frac{k_B T_c}{a}$, where the terms k_B, T_c and a are Boltzmann constant, Curie Temperature and lattice parameter, respectively. We found A_{ex} about 26 $\frac{pJ}{m}$, which is in the same order as reported in the literature [23]. The equilibrium states were obtained by fully relaxing the randomly distributed magnetization. Figures 7.4[i-vi] show the simulated spin-textures at different values of applied out-of-plane external magnetic fields. At zero magnetic field, we observed the opposite aligned magnetic strip domains as shown in Fig.7.4(i). With increasing the magnetic field strip domains shrink

and start to break into circular magnetic domains (often called skyrmionic bubbles/dipole-stabilized skyrmion) at the field value of 0.2 T [Fig.7.4(iii)]. The observed skyrmionic bubbles possess Bloch-type dynamics and are stable up to a field of 0.4 T [Fig.7.4(v)]. On further increasing the magnetic field to the 0.5 T the circular magnetic domains collapse into the spin-polarized state [Fig.7.4(vi)]. The disappearance of skyrmion at 0.5 T in the micromagnetic simulation, in contrast to the experimental vanishing of ρ^T around 1 T might be due to the difference in sizes of the domain structure between the simulated and real case of material [10, 71]. Simulating a larger cell to match real-world conditions would be computationally expensive and therefore not practical [71]. To calculate the winding number (S), we have chosen the slab geometry of 250 nm $\times$ 250 nm $\times$ 80 nm with a cell size of 5 nm $\times$ 5 nm $\times$ 2 nm such that a single skyrmion would nucleate in the slab. We found the value of $S \approx$ -0.95 which is close to 1 that supports the formation of skyrmions in the present system. To further confirm the topology of skyrmion we plotted the side view (not shown here) of the spin texture at 0.4 T and found that the +m_z (red color) and -m_z (blue color) states are opposite to each other with respect to the center (*i.e.* helicity $\gamma=\pi/2$), which also precludes S=0 for the observed skyrmionic bubble in the system. Therefore, the observed THE in the present system is related to the skyrmions developed by competition among the magneto-crystalline anisotropy, exchange interaction, and long-range dipolar interactions. Our work presents a new opportunity to explore THE associated with real space Berry curvature originated from the skyrmionic structure of the bulk centrosymmetric material. It would be assuming the further observation of real or reciprocal space images of skyrmion texture in the present system.

7.3 Conclusion

To conclude, we studied THE in the bulk Co_2FeAl Heusler compound through magnetotransport measurements. We found that THE stabilizes in a wide temperature range (2 K to 300 K), with a maximum value of 0.22 $\mu\Omega$-cm at 300K. The THE varies rather slowly with temperature suggesting its correlation with the skyrmions present in the compound. Furthermore, the hump anomaly in AC-$\chi(H)$ measurement, which aligns with the field where THE reaches its peak, provides further evidence of skyrmion formation in this system. The micromagnetic simulations demonstrate the emergence of a skyrmionic state resulting from competition among magnetic anisotropy, ex-

change interaction, and dipolar interactions. This study presents indirect evidence of the signature of skyrmions and triggers the additional observation through Lorentz transmission electron microscopy (LTEM) or diffraction studies in the future. Owing to the high Curie temperature and significant THE, this material is useful for potential technological applications at room temperature as well as high temperatures.

References

[1] N. Nagaosa and Y. Tokura, Topological properties and dynamics of magnetic skyrmions, Nat. Nanotechnol **8**, 899 (2013).

[2] M. B. Jalil and S. G. Tan, Robustness of topological Hall effect of nontrivial spin textures, Sci. Rep. **4**, 5123 (2014).

[3] B. Göbel, I. Mertig, and O. A. Tretiakov, Beyond skyrmions: Review and perspectives of alternative magnetic quasiparticles, Phys. Rep. **895**, 1 (2021).

[4] B. Göbel and I. Mertig, Quaternary-digital data storage based on magnetic bubbles in anisotropic materials, Phys. Rev. Appl. **15**, 064052 (2021).

[5] Y. He, S. Schneider, T. Helm, J. Gayles, D. Wolf, I. Soldatov, H. Borrmann, W. Schnelle, R. Schaefer, G. H. Fecher, *et al.*, Topological Hall effect arising from the mesoscopic and microscopic non-coplanar magnetic structure in MnBi, Acta Mater. **226**, 117619 (2022).

[6] M. Raju, A. Petrović, A. Yagil, K. Denisov, N. Duong, B. Göbel, E. Şaşıoğlu, O. Auslaender, I. Mertig, I. Rozhansky, *et al.*, Colossal topological Hall effect at the transition between isolated and lattice-phase interfacial skyrmions, Nat. Commun. **12**, 2758 (2021).

[7] M. Huang, L. Gao, Y. Zhang, X. Lei, G. Hu, J. Xiang, H. Zeng, X. Fu, Z. Zhang, G. Chai, *et al.*, Possible topological Hall effect above room temperature in layered $Cr_1.2Te_2$ ferromagnet, Nano Lett. **21**, 4280 (2021).

[8] S.-S. Zhang, H. Ishizuka, H. Zhang, G. B. Halász, and C. D. Batista, Real-space Berry curvature of itinerant electron systems with spin-orbit interaction, Phys. Rev. B **101**, 024420 (2020).

[9] V. Kumar, G. K. Shukla, N. Shahi, and S. Singh, Topological Hall effect in $(Mn_{1-x}Fe_x)_{3.25}Ge$ (x= 0.4) hexagonal magnet, Phys. Status Solidi - Rapid Res. Lett. **17**, 2300174 (2023).

[10] S. Rastogi, N. Shahi, V. Kumar, G. K. Shukla, S. Bhattacharjee, and S. Singh, Revealing the origin of the topological Hall effect in the centrosymmetric shape memory Heusler alloy Mn_2NiGa: A combined experimental and theoretical investigation, Phys. Rev. B **108**, 224108 (2023).

[11] Q. Shao, Y. Liu, G. Yu, S. K. Kim, X. Che, C. Tang, Q. L. He, Y. Tserkovnyak, J. Shi, and K. L. Wang, Topological Hall effect at above room temperature in heterostructures composed of a magnetic insulator and a heavy metal, Nat. Electron **2**, 182 (2019).

[12] P. Bruno, V. K. Dugaev, and M. Taillefumier, Topological Hall effect and Berry phase in magnetic nanostructures, Phys. Rev. Lett. **93**, 096806 (2004).

[13] W. Wang, Y. Zhang, G. Xu, L. Peng, B. Ding, Y. Wang, Z. Hou, X. Zhang, X. Li, E. Liu, *et al.*, A centrosymmetric hexagonal magnet with superstable biskyrmion magnetic nanodomains in a wide temperature range of 100–340 K, Adv. Mater. **28**, 6887 (2016).

[14] W. Jiang, P. Upadhyaya, W. Zhang, G. Yu, M. B. Jungfleisch, F. Y. Fradin, J. E. Pearson, Y. Tserkovnyak, K. L. Wang, O. Heinonen, *et al.*, Blowing magnetic skyrmion bubbles, Science **349**, 283 (2015).

[15] A. Fert, N. Reyren, and V. Cros, Magnetic skyrmions: advances in physics and potential applications, Nat. Rev. Mater. **2**, 17031 (2017).

[16] C. Felser and S. Parkin, Topology, Skyrmions, and Heusler compounds, MRS Bulletin **47**, 600 (2022).

[17] A. Fert, V. Cros, and J. Sampaio, Skyrmions on the track, Nat. Nanotechnol **8**, 152 (2013).

[18] X. Yu, Y. Tokunaga, Y. Taguchi, and Y. Tokura, Variation of topology in magnetic bubbles in a colossal magnetoresistive manganite, Adv. Mater. **29**, 1603958 (2017).

[19] S. Li, X. Wang, and T. Rasing, Magnetic skyrmions: Basic properties and potential applications, Interdiscip. Mater. **2**, 260 (2023).

[20] S. Mühlbauer, B. Binz, F. Jonietz, C. Pfleiderer, A. Rosch, A. Neubauer, R. Georgii, and P. Böni, Skyrmion lattice in a chiral magnet, Science **323**, 915 (2009).

[21] X. Yu, N. Kanazawa, Y. Onose, K. Kimoto, W. Zhang, S. Ishiwata, Y. Matsui, and Y. Tokura, Near room-temperature formation of a skyrmion crystal in thin-films of the helimagnet FeGe, Nat. Mater **10**, 106 (2011).

[22] X. Yu, Y. Onose, N. Kanazawa, J. Park, J. Han, Y. Matsui, N. Nagaosa, and Y. Tokura, Real-space observation of a two-dimensional skyrmion crystal, Nat. **465**, 901 (2010).

[23] S. Husain, N. Sisodia, A. K. Chaurasiya, A. Kumar, J. P. Singh, B. S. Yadav, S. Akansel, K. H. Chae, A. Barman, P. Muduli, *et al.*, Observation of skyrmions at room temperature in Co_2FeAl Heusler alloy ultrathin film heterostructures, Sci. Rep. **9**, 1085 (2019).

[24] C. Moreau-Luchaire, C. Moutafis, N. Reyren, J. Sampaio, C. Vaz, N. Van Horne, K. Bouzehouane, K. Garcia, C. Deranlot, P. Warnicke, *et al.*, Additive interfacial chiral interaction in multilayers for stabilization of small individual skyrmions at room temperature, Nat. Nano. **11**, 444 (2016).

[25] A. Soumyanarayanan, M. Raju, A. Gonzalez Oyarce, A. K. Tan, M.-Y. Im, A. P. Petrović, P. Ho, K. Khoo, M. Tran, C. Gan, *et al.*, Tunable room-temperature magnetic skyrmions in Ir/Fe/Co/Pt multilayers, Nat. Mater. **16**, 898 (2017).

[26] S. Woo, K. Litzius, B. Krüger, M.-Y. Im, L. Caretta, K. Richter, M. Mann, A. Krone, R. M. Reeve, M. Weigand, *et al.*, Observation of room-temperature magnetic skyrmions and their current-driven dynamics in ultrathin metallic ferromagnets, Nat. Mater. **15**, 501 (2016).

[27] S. Sen, C. Singh, P. K. Mukharjee, R. Nath, and A. K. Nayak, Observation of the topological Hall effect and signature of room-temperature antiskyrmions in Mn-Ni-Ga D_2d Heusler magnets, Phys. Rev. B **99**, 134404 (2019).

[28] A. K. Srivastava, P. Devi, A. K. Sharma, T. Ma, H. Deniz, H. L. Meyerheim, C. Felser, and S. S. Parkin, Observation of robust Neel skyrmions in metallic PtMnGa, Adv. Mater. **32**, 1904327 (2020).

[29] L. Peng, R. Takagi, W. Koshibae, K. Shibata, K. Nakajima, T.-h. Arima, N. Nagaosa, S. Seki,

X. Yu, and Y. Tokura, Controlled transformation of skyrmions and antiskyrmions in a non-centrosymmetric magnet, Nat. Nano. **15**, 181 (2020).

[30] K. Rana, O. Meshcheriakova, J. Kübler, B. Ernst, J. Karel, R. Hillebrand, E. Pippel, P. Werner, A. Nayak, C. Felser, *et al.*, Observation of topological hall effect in Mn_2RhSn films, New J. Phys. **18**, 085007 (2016).

[31] O. Meshcheriakova, S. Chadov, A. Nayak, U. Rößler, J. Kübler, G. André, A. Tsirlin, J. Kiss, S. Hausdorf, A. Kalache, *et al.*, Large noncollinearity and spin reorientation in the novel Mn_2RhSn Heusler magnet, Phys. Rev. Lett. **113**, 087203 (2014).

[32] T. Okubo, S. Chung, and H. Kawamura, Multiple-q states and the skyrmion lattice of the triangular-lattice Heisenberg antiferromagnet under magnetic fields, Phys. Rev. Lett. **108**, 017206 (2012).

[33] D. Chakrabartty, S. Jamaluddin, S. K. Manna, and A. K. Nayak, Tunable room temperature magnetic skyrmions in centrosymmetric kagome magnet Mn_4Ga_2Sn, Communications Physics **5**, 189 (2022).

[34] M. Altthaler, E. Lysne, E. Roede, L. Prodan, V. Tsurkan, M. A. Kassem, H. Nakamura, S. Krohns, I. Kézsmárki, and D. Meier, Magnetic and geometric control of spin textures in the itinerant kagome magnet Fe_3Sn_2, Phys. Rev. Res. **3**, 043191 (2021).

[35] J. Tang, L. Kong, Y. Wu, W. Wang, Y. Chen, Y. Wang, J. Li, Y. Soh, Y. Xiong, M. Tian, *et al.*, Target bubbles in Fe_3Sn_2 nanodisks at zero magnetic field, ACS nano **14**, 10986 (2020).

[36] J. A. Paddison, B. K. Rai, A. F. May, S. Calder, M. B. Stone, M. D. Frontzek, and A. D. Christianson, Magnetic interactions of the centrosymmetric skyrmion material Gd_2PdSi_3, Phys. Rev. Lett. **129**, 137202 (2022).

[37] T. Kurumaji, T. Nakajima, M. Hirschberger, A. Kikkawa, Y. Yamasaki, H. Sagayama, H. Nakao, Y. Taguchi, T.-h. Arima, and Y. Tokura, Skyrmion lattice with a giant topological Hall effect in a frustrated triangular-lattice magnet, Science **365**, 914 (2019).

[38] S. Montoya, S. Couture, J. Chess, J. Lee, N. Kent, D. Henze, S. Sinha, M.-Y. Im, S. Kevan,

P. Fischer, *et al.*, Tailoring magnetic energies to form dipole skyrmions and skyrmion lattices, Phys. Rev. B **95**, 024415 (2017).

[39] B. Ding, Z. Li, G. Xu, H. Li, Z. Hou, E. Liu, X. Xi, F. Xu, Y. Yao, and W. Wang, Observation of magnetic skyrmion bubbles in a van der waals ferromagnet Fe_3GeTe_2, Nano letters **20**, 868 (2019).

[40] B. Ding, J. Cui, G. Xu, Z. Hou, H. Li, E. Liu, G. Wu, Y. Yao, and W. Wang, Manipulating spin chirality of magnetic skyrmion bubbles by in-plane reversed magnetic fields in $(Mn_{(1-x)}Ni_x)_{65}Ga_{35}$(x= 0.45) magnet, Phys. Rev. Appl. **12**, 054060 (2019).

[41] K. Inomata, N. Ikeda, N. Tezuka, R. Goto, S. Sugimoto, M. Wojcik, and E. Jedryka, Highly spin-polarized materials and devices for spintronics, Sci. Technol. Adv. **9**, 014101 (2008).

[42] K. Elphick, W. Frost, M. Samiepour, T. Kubota, K. Takanashi, H. Sukegawa, S. Mitani, and A. Hirohata, Heusler alloys for spintronic devices: review on recent development and future perspectives, Sci. Technol. Adv. Mate **22**, 235 (2021).

[43] T. Graf, C. Felser, and S. S. Parkin, Simple rules for the understanding of Heusler compounds, Prog. Solid. State Ch. **39**, 1 (2011).

[44] C. Phatak, O. Heinonen, M. De Graef, and A. Petford-Long, Nanoscale skyrmions in a nonchiral metallic multiferroic: Ni_2MnGa, Nano Lett. **16**, 4141 (2016).

[45] J. C. Loudon, A. C. Twitchett-Harrison, D. Cortés-Ortuño, M. T. Birch, L. A. Turnbull, A. Štefančič, F. Y. Ogrin, E. O. Burgos-Parra, N. Bukin, A. Laurenson, *et al.*, Do images of biskyrmions show type-ii bubbles?, Adv. Mater. **31**, 1806598 (2019).

[46] W. Zhang, B. Balasubramanian, A. Ullah, R. Pahari, X. Li, L. Yue, S. R. Valloppilly, A. Sokolov, R. Skomski, and D. J. Sellmyer, Comparative study of topological Hall effect and skyrmions in NiMnIn and NiMnGa, Appl. Phys. Lett. **115**, 172404 (2019).

[47] X. Zhang, H. Xu, B. Lai, Q. Lu, X. Lu, Y. Chen, W. Niu, C. Gu, W. Liu, X. Wang, *et al.*, Direct observation of high spin polarization in Co_2FeAl thin films, Sci. Rep. **8**, 8074 (2018).

[48] S. Husain, S. Akansel, A. Kumar, P. Svedlindh, and S. Chaudhary, Growth of Co_2FeAl Heusler

alloy thin films on Si (100) having very small gilbert damping by ion beam sputtering, Sci. Rep. **6**, 28692 (2016).

[49] G. K. Shukla, A. K. Jena, N. Shahi, K. K. Dubey, I. Rajput, S. Baral, K. Yadav, K. Mukherjee, A. Lakhani, K. Carva, S.-C. Lee, S. Bhattacharjee, and S. Singh, Atomic disorder and Berry phase driven anomalous Hall effect in a Co_2FeAl Heusler compound, Phys. Rev. B **105**, 035124 (2022).

[50] W. Akhtar, A. Hrabec, S. Chouaieb, A. Haykal, I. Gross, M. Belmeguenai, M. Gabor, B. Shields, P. Maletinsky, A. Thiaville, *et al.*, Current-induced nucleation and dynamics of skyrmions in a Co-based Heusler alloy, Phys. Rev. Appl. **11**, 034066 (2019).

[51] M. Kogachi, N. Tadachi, and T. Nakanishi, Structural properties and magnetic behavior in $CoFe_{1-x}Al_x$ alloys, Intermetallics **14**, 742 (2006).

[52] S. Wurmehl, G. H. Fecher, K. Kroth, F. Kronast, H. A. Dürr, Y. Takeda, Y. Saitoh, K. Kobayashi, H.-J. Lin, G. Schönhense, *et al.*, Electronic structure and spectroscopy of the quaternary Heusler alloy $Co_2Cr_{1-x}Fe_xAl$, Journal of Physics D: Applied Physics **39**, 803 (2006).

[53] N. Shahi, A. K. Jena, G. K. Shukla, V. Kumar, S. Rastogi, K. K. Dubey, I. Rajput, S. Baral, A. Lakhani, S.-C. Lee, S. Bhattacharjee, and S. Singh, Antisite disorder and Berry curvature driven anomalous Hall effect in the spin gapless semiconducting Mn_2CoAl Heusler compound, Phys. Rev. B **106**, 245137 (2022).

[54] S. Trudel, O. Gaier, J. Hamrle, and B. Hillebrands, Magnetic anisotropy, exchange and damping in Cobalt-based full-Heusler compounds: an experimental review, J. Phys. D: Appl. Phys. **43**, 193001 (2010).

[55] A. K. Singh, G. K. Shukla, and S. Singh, Intrinsic anomalous Hall conductivity and real space Berry curvature induced topological Hall effect in Ni_2MnGa magnetic shape memory alloy, J. Phys. D: Appl. Phys **56**, 044004 (2022).

[56] J. F. Herbst and F. E. Pinkerton, Law of approach to saturation for polycrystalline ferromagnets: Remanent initial state, Phys. Rev. B **57**, 10733 (1998).

[57] X. Li, S. Yin, Y. Liu, D. Zhang, X. Xu, J. Miao, and Y. Jiang, Perpendicular magnetic anisotropy of full-Heusler films in Pt/Co_2FeAl/MgO trilayers, Appl. Phys. Express. **4**, 043006 (2011).

[58] M. He, G. Li, Z. Zhu, Y. Zhang, L. Peng, R. Li, J. Li, H. Wei, T. Zhao, X.-G. Zhang, *et al.*, Evolution of topological skyrmions across the spin reorientation transition in Pt/Co/Ta multi-layers, Phys. Rev. B **97**, 174419 (2018).

[59] G. K. Shukla, J. Sau, N. Shahi, A. K. Singh, M. Kumar, and S. Singh, Anomalous Hall effect from gapped nodal line in the Co_2FeGe Heusler compound, Phys. Rev. B **104**, 195108 (2021).

[60] G. K. Shukla, J. Sau, V. Kumar, M. Kumar, and S. Singh, Band splitting induced Berry flux and intrinsic anomalous Hall conductivity in the NiCoMnGa quaternary heusler compound, Phys. Rev. B **106**, 045131 (2022).

[61] X.-Z. Li, W.-Y. Zhang, S. Valloppilly, and D. J. Sellmyer, New Heusler compounds in Ni-Mn-In and Ni-Mn-Sn alloys, Sci. Rep. **9**, 7762 (2019).

[62] M. Leroux, M. J. Stolt, S. Jin, D. V. Pete, C. Reichhardt, and B. Maiorov, Skyrmion lattice topological Hall effect near room temperature, Sci. Rep. **8**, 15510 (2018).

[63] A. Hrabec, J. Sampaio, M. Belmeguenai, I. Gross, R. Weil, S. M. Chérif, A. Stashkevich, V. Jacques, A. Thiaville, and S. Rohart, Current-induced skyrmion generation and dynamics in symmetric bilayers, Nat. Commun. **8**, 15510 (2017).

[64] X. Xiao, L. Peng, X. Zhao, Y. Zhang, Y. Dai, J. Guo, M. Tong, J. Li, B. Li, W. Liu, *et al.*, Low-field formation of room-temperature biskyrmions in centrosymmetric MnPdGa magnet, Appl. Phys. Lett. **114**, 142404 (2019).

[65] M. Blinov, V. Chernenko, V. Prudnikov, I. Aseguinolaza, J. Barandiaran, E. Lahderanta, and A. Granovsky, Anomalous Hall effect in $Ni_{47.3}Mn_{30.6}Ga_{22.1}$/MgO(001) thin films, Phys. Rev. B **102**, 064413 (2020).

[66] M. Maus, *AC Susceptometry for Characterizing Magnetic Spin Structures*, Ph.D. thesis, University of Colorado, Boulder (2019).

[67] S. Sen, C. Singh, P. K. Mukharjee, R. Nath, and A. K. Nayak, Observation of the topological Hall effect and signature of room-temperature antiskyrmions in Mn-Ni-Ga D_{2d} Heusler magnets, Phys. Rev. B **99**, 134404 (2019).

[68] S. Jamaluddin, S. K. Manna, B. Giri, P. P. Madduri, S. S. Parkin, and A. K. Nayak, Robust antiskyrmion phase in bulk tetragonal Mn-Pt (Pd)-Sn Heusler system probed by magnetic entropy change and AC-susceptibility measurements, Adv. Funct. Mater. **29**, 1901776 (2019).

[69] S. Seki, X. Yu, S. Ishiwata, and Y. Tokura, Observation of skyrmions in a multiferroic material, Science **336**, 198 (2012).

[70] D. Porter, M. Donahue, R. McMichael, and J. Blue, Oommf: Public domain micromagnetic software, in *1998 IEEE International Magnetics Conference (INTERMAG)* (IEEE, 1998) pp. 113–113.

[71] A. Mourkas, A. Markou, P. Swekis, and I. Panagiotopoulos, Topological Hall effect in Pt/-Co/W multilayers with different anisotropies, J. Magn. Magn. Mater. **530**, 167937 (2021).